Journal of Structural Geology, Vol. 5, No. 3/4, pp. 383 to 399, 1983
Printed in Great Britain

0191-8141/83 $3.00 + 0.00

Complex strain patterns developed at the frontal and lateral tips to shear zones and thrust zones

M. P. COWARD and G. J. POTTS

Department of Earth Sciences, University of Leeds, Leeds LS2 9JT, England

(*Received* 21 *June* 1982; *accepted in revised form* 8 *November* 1982)

Abstract—Many of the complex strain patterns seen in shear zones and thrust zones, such as variable fabric orientations, refolded folds and fabrics, together with folds with hinges almost parallel to the main transport direction, can be explained in terms of differential movement within the shear zones. These strains are developed at the frontal and lateral tips of the zones as they propagate. Examples are taken from the Moine thrust zone of Scotland which show variations in strains particularly at the lateral tips. The form of differential movement described here may lead to complex strain paths and non-plane strain ellipsoids and the spatial variations in finite strain may be used to delineate zones of extensional and compressional flow and differential movement in the shear zones or thrusts.

TIPS TO THRUST AND SHEAR ZONES

IF THRUST surfaces and shear zones are considered to propagate from instabilities at the boundaries of a mass of rock, as suggested by Douglas (1958) and Elliott (1976) then at the tips of these propagating zones the rocks must suffer strain related to this propagation. These strains may be elastic, and hence completely recoverable, but there is growing evidence for the existence of permanent plastic deformation at the tips of thrusts and shear zones. The aim of this paper is to discuss the geometry of these tip strains, particularly in high-crustal-level thin-skinned thrust zones and also in deeper-level more ductile shear zones.

Figure 1 shows a sketch of a gently dipping bedding-parallel thrust plane and the adjacent rock. The bedding may be divided into that part which has slipped and that part into which the thrust may propagate. The slipped thrust plane may be considered similar to a dislocation glide plane in a crystal structure. The strain at the tip depends on the amount of movement in the slipped region and the width of the tip. The tips may be frontal, analogous to edge dislocations, or lateral, analogous to screw dislocations. Thus in thrust zones we should expect compressive strains or layer-parallel shortening at the frontal tips and shear strains at the lateral tips. These shear strains will be developed with shear planes normal to the main thrust plane but with the same transport direction. Some fault zones involve both contractional (thrust) faults and extensional (low angle normal) faults (Coward 1982). These zones of extensional faults are considered to propagate in the opposite direction to fault movement, leading to the production of extensional strains at the tips. Many deeper level ductile shear zones and thrust zones which develop from some instability in a rock system must have frontal, rear and lateral tips.

Many thrust sheets show no internal deformation (cf. McClay & Coward 1981) and the thrust beneath must have been able to propagate easily, the tip zone moving rapidly through the rock. Other thrust zones, however, show bedding-parallel longitudinal strains and evidence of up to 30% bed thickening (Coward & Kim 1981, Cooper *et al.* 1983). Cooper *et al.* consider that thrusts often develop a ductile bead of permanent deformation ahead of the slipped zone. However, Fischer & Coward (1982) report that in the Moine Thrust Zone, the layer-parallel shortening is often patchy and that in the Eriboll district (Figs. 2 and 3) there are localized zones of more intense layer-parallel shortening. It appears that the ease of thrust propagation may vary for a particular thrust plane and that locally high strains may be produced at a thrust tip. This layer-parallel shortening may cause the rocks to fold; the folds produced are often asymmetric with a more intensely strained overturned limb. Often the folds have been cut through by a thrust plane which developed from the flat beneath the fold. Presumably the thrust found it easier to break through the more highly strained limb, than continue along the original decoupling horizon to the fold. With further movement on this new inclined thrust the anticlinal structure may be carried some distance ahead of the syncline in the footwall (Fig. 4). These thrust and buckle folds may be distinguished from the structurally necessary folds formed by a stair-step thrust trajectory (Rich

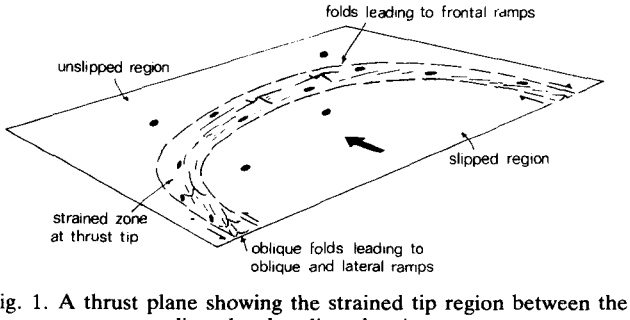

Fig. 1. A thrust plane showing the strained tip region between the slipped and unslipped regions.

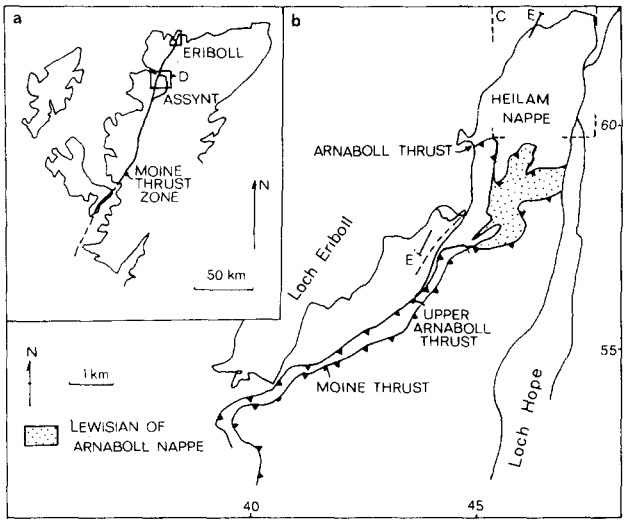

Fig. 2. (a) Locality map for the Moine thrust zone of NW Scotland. (b) Locality map for the Heilam nappe, Loch Eriboll, outlined in (a).

1934, Harris & Milici 1977) by the high strains on the steep to inverted limb, the tight interlimb angle, the presence of folds in the footwall, parasitic folds and the presence of layer-parallel shortening strain on the bedding surface. The intense strain and fold zone, therefore, forms the development site of a new thrust and becomes what is termed a *branch line* rather than a thrust *tip*. Within many thrust zones, such as the Moine, tip lines are rarely preserved; most have developed into frontal or lateral branch lines.

At the lateral tips, the thrusts often die out along strike into folds. Elliott (1976) produced a model of fault development where a non-cylindrical fold complex travels just ahead of a sideways-propagating thrust. The rocks would fold, the folds grow and tighten and the thrust fault extend into the deformed rock, slicing through the intensely sheared overturned limb to make a 'forelimb thrust' or the less sheared right-way-up limb to make a 'backlimb thrust' (Douglas 1958). The folds described by Elliott (1976) from the Rockies Foothills and Ranges generally die out about 9 km from the ends of the thrusts. It is thought that lateral tips of this type propagate at approximately ten times the thrust displacement rate.

Not all thrusts climb through the cores of folds; most imbricate faults climb through relatively unstrained and unfolded strata. They presumably developed where the stress build-up was rapid enough for failure to occur before plastic deformation, producing a plane cutting up obliquely through the beds. Such local build-ups of stress presumably occur at thrust tips where thrust propagation becomes more difficult. This change in ease of propagation may occur where there are variations in rock type or fluid pressure along a particular thrust plane causing variations in cohesion and friction. The slipped zone may overlie an area of sufficiently high fluid pressure to ease fault propagation and movement while the unslipped region may overlie a zone of low fluid pressure and hence a stress build-up. Thus ductile strain will occur at the tip between the two zones, where the fault sticks.

The strain associated with thrust faulting may be due to the propagation of the thrust tip, as a ductile bead moving ahead of the slipped region. However the more intense strains develop at the tips where the fault sticks and these more intensely deformed zones often develop into branch lines.

In the Eriboll area of Scotland (Figs. 3 and 4), strain ellipses on the bedding are generally orientated almost perpendicular to the thrust transport direction and are therefore considered to be related to frontal tips, leading to the development of branch lines. The rocks are Cambrian quartzites, dolomitic mudstones, grits and limestones involved in the lower thrust sheets of the Moine thrust zone (Peach *et al.* 1907, McClay & Coward 1980). The strains are recorded by deformed pipes (genus *Skolithus*) which originally had approximately circular sections on the bedding planes. Some of the strain ratios and orientations are shown in Fig. 3(b) (after Fischer & Coward 1982). Throughout most of the area the ellipses are orientated NNE–SSW, normal to the transport direction, but in some areas ellipses are oblique, suggesting that here there has also been a component of shear strain on the bedding surface, as would be produced in the region of a lateral tip. The strains have been factorized into components of layer-parallel shortening ($\sqrt{\lambda}$), as would be formed at a frontal tip and layer-normal shear (γ_2) as would be found at a lateral tip. The results, given in detail in Fischer & Coward (1982) suggest that only slight (γ_2) shear strains occur, except in the north, where the ellipses' long axes trend NE–ENE. In this area the γ_2 component reaches values of 0.4 with dextral sense. The imbricate faults and related folds generally trend NNE, normal to the transport direction, but to the south the imbricate faults are oblique and locally steepen up the beds in oblique to lateral hanging-wall ramps (Fig. 5). These folds are probably not due to buckling but were formed by close spacing of the lateral fault branch lines. Thus in the south there are relatively few thrust faults but to the north these branch into numerous imbricate thrusts. In the southern part of the Heilam thrust sheet, the displacement on the faults apparently does not decrease but the faults join together, transferring movement to a single thrust plane. Whether or not these lateral ramps are due to sticking processes at lateral tips is not known. In the northern part of the Heilam sheet, however, the displacement decreases producing locally intense lateral tip shear strains. In this northern area no oblique folds were produced.

At Assynt (Fig. 4a), there are lateral thrust ramps and oblique folds but here many of the folds are due to a buckling process and the strain ellipses on the bedding planes, shown by deformed sections of pipes, are oblique to the transport direction and also oblique to the fold traces. Coward & Kim (1981) factorized the ellipses into components of layer-parallel shortening and differential sinistral movement and recorded sinistral shear strains of up to 0.6. This northern Assynt region seems to have

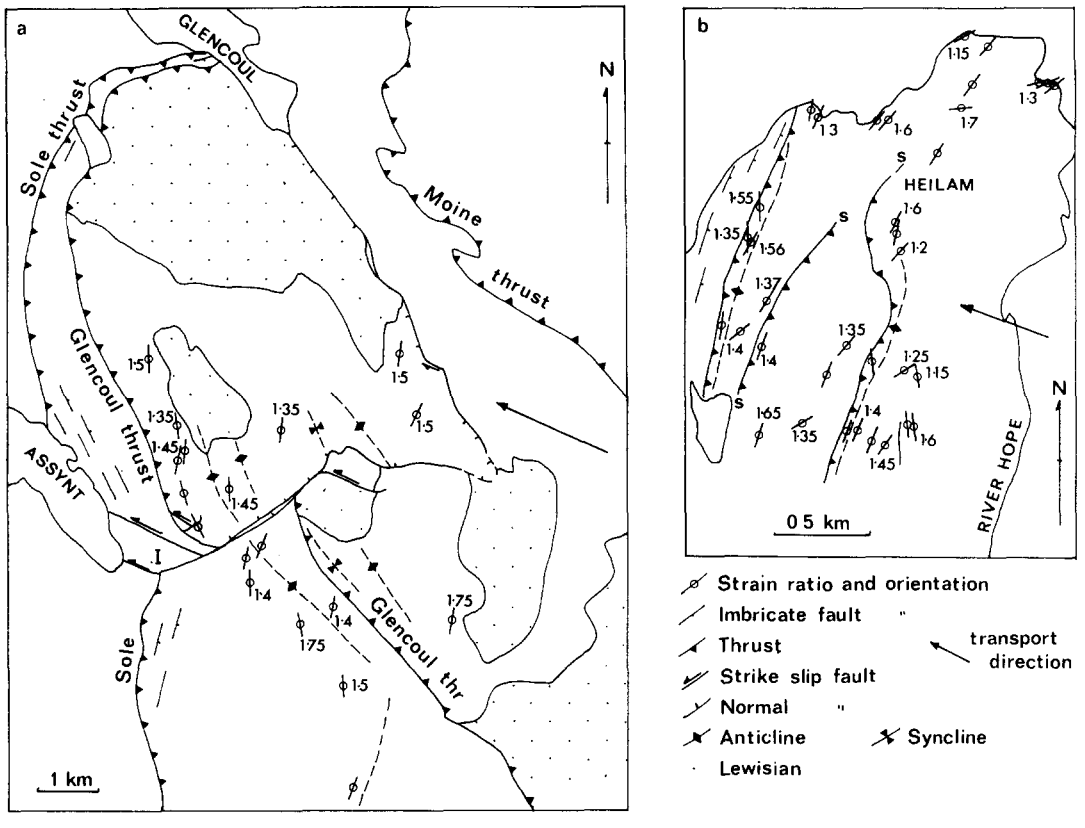

Fig. 3. (a) Orientations of strain ellipses and a few strain ratios from the north Assynt area showing the oblique nature of the strains, after Coward & Kim (1981). Location shown by D in Fig. 2(a). The strains were measured from the originally near-circular sections of pipes on the bedding planes. (b) Strain ratios and orientations from deformed Pipe Rock from the Heilam thrust sheet of the Eriboll area. Location shown in Fig. 2(b), after Fischer & Coward (1982). The terminations of the faults on the map (marked s) show where the faults lose stratigraphic separation and are difficult to detect in the field.

been the locus for several lateral thrust tips, not leading just to lateral ramps as in Eriboll, but also to permanent strains in the rock and the development of asymmetric buckle folds.

In their analysis of ductile shear zones, Ramsay & Graham (1970) showed that the displacements within a zone were due to progressive simple shear with or without volume change. If the surrounding material is undeformed or homogeneously deformed, no other strains can be compatible (Ramsay & Graham 1970). However in some shear zones, where the strain can be measured, the finite strains are not due to simple shear or volume change alone (Coward 1976). Figure 6 shows strain ratios plotted against orientations for sheared metadolerite from Castell O'dair, North Uist, Scotland, where the strain measurements were made from clots of mafic and felsic material. The rock from which these measurements were taken has no discernible fabric outside the zone and the anomalous strains, therefore, cannot be due to the superimposition of a shear strain on a regional homogeneous or heterogeneous strain field. There is no evidence for volume change within the zone, no obvious change in petrology of the rocks and if volume change was the sole deformation mechanism apart from simple shear, then there would be volume increase in one part of the zone, volume decrease in another part. It is considered that these zones depart from true simple-shear geometry and the finite strain contains small components of layer-parallel shortening or elongation, probably caused by differential movement of the zone.

Coward (1976) reported such non-simple-shear strains from termination zones or tips to shear zones but also recorded some from near the centres of the zones. In

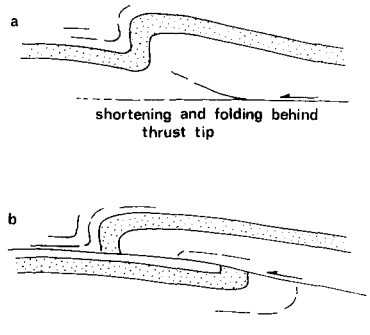

Fig. 4. Model for the production of folds and thrusts in the Eriboll and Assynt areas. (a) The rocks are shortened and folded in the thrust tip zone. This causes crumpling and intense strains on the inner arcs of the folds, often producing 'out of syncline' thrusts. There may also be intense strains on the steeper fold limb due to flexural slip processes. (b) A thrust fault propagates through the intensely deformed zone carrying the antiform some distance from the syncline in the footwall. Note, the folds do not always verge in the thrust transport direction. In the Assynt area the folds are locally more symmetric and sometimes face in the opposite direction to transport. Some of the resulting thrusts are thus back-thrusts with movement opposite to that of the main thrust system.

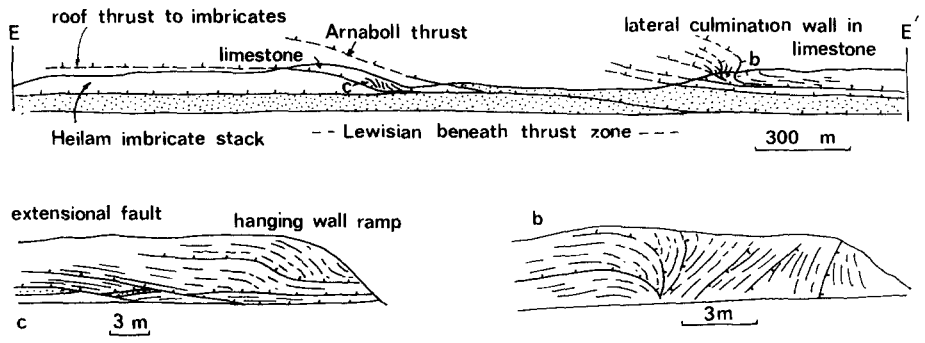

Fig. 5. Section parallel to the strike of the thrust belt at Eriboll. For location see Fig. 2(b). Many of the thrusts in the northern part of the section join together, transferring displacement to relatively few thrust faults in the south. (b) and (c) are details of this section. Note that where lateral ramps are closely spaced, as in (b), large asymmetric folds may be produced which are superficially similar to lateral tip folds produced by buckling.

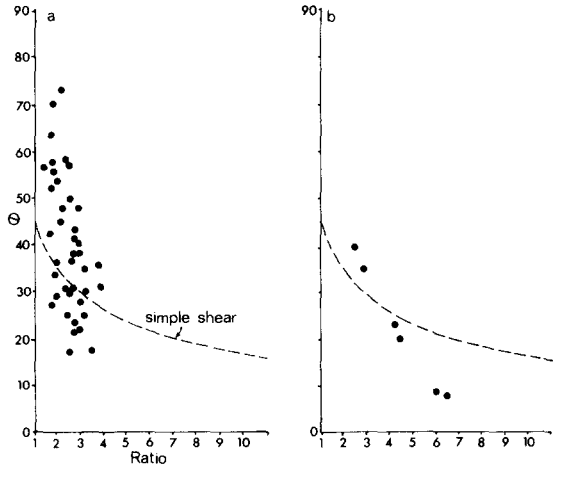

Fig. 6. Strain ratios, plotted against orientation θ from the shear plane for (a) a shear zone which cuts unfoliated metadolerite from N.E. Botswana—after Coward (1976) and (b) a shear zone which cuts otherwise unfoliated metadolerite, Castell O'dair, North Uist, Scotland.

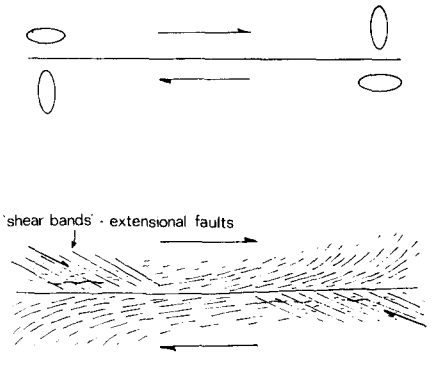

Fig. 7. Second order shear zones or 'shear bands' formed in the zones of extensional strain at the tips of shear zones.

these latter examples, the non-simple shear strains may have formed early, at the tips of the initial shear zone and then have been modified by simple-shear strains as the shear zone propagated. It is possible, however, that they may also be due to differential movement late in the shear zone history. The strain path is unknown.

Extensional flow at the ends or within the shear zone may give rise to second-order structures (Fig. 7), termed extensional crenulation cleavage by Platt & Vissers (1980) and shear bands by White (1980). They presumably form by the compression of an anisotropic medium (Cobbold *et al.* 1971). In zones of co-axial deformation, two sets of shears are produced, conjugate about the layering. In non-coaxial zones, such as shear zones, only one set is produced, with the same sense of movement as the main shear (Platt & Vissers 1980). The wide extent of these bands in the Hercynian shear zones of Brittany (Berthé *et al.* 1979) and North Spain (Ponce de Leon & Choukroune 1980) attests to the wide extent of extensional flow in these zones.

Compressional flow at the end of a shear zone may cause local folding; Fig. 8 gives an example from the Farhead Point shear, in the Lewisian rocks of NW Scotland. Compressional flow within shear zones may cause localized folding of earlier shear-zone fabrics. This compressional flow may occur near the tips to a later wave of shear movement affecting the zone. Cobbold & Quinquis (1980) have shown that only small perturbations of the fabric are required to produce folds in shear zones. Several phases of such folds, with curvilinear hinges, were produced in the laboratory by Cobbold & Quinquis (1980) by the shearing of layered models with small induced perturbations. In nature, one possible mechanism to produce such perturbations of the shear plane may be small localized components of layer-parallel shortening or extension.

DISPLACEMENTS IN SHEAR ZONES

The concept of strain paths

Deformation paths define the history of deformation. Generally the path by which the incremental strains build up to a large finite strain is complex. For some specific deformations, however, such as those which produce a finite pure shear or finite simple shear we often know or can assume the incremental strain history and the rotation rate or vorticity of the principal strains.

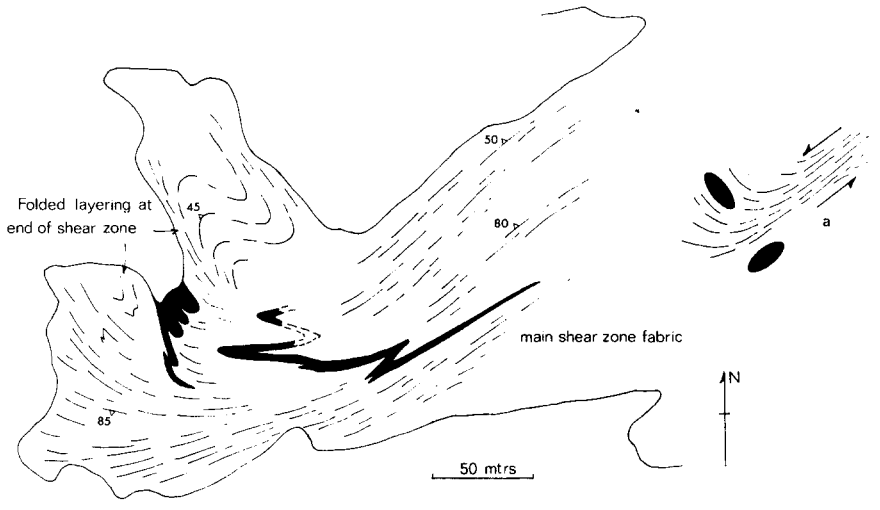

Fig. 8. Sketch map of a shear zone which cuts Lewisian Gneiss at Farhead Point, Badcall, near Scourie, Sutherland (see also Beach, in Barber *et al.* 1978, p. 19). The black zone represents a deformed Scourie dyke in Lewisian gneiss. The lines represent foliation trends in the gneiss. (a) shows an idealized model for the strains in this shear zone.

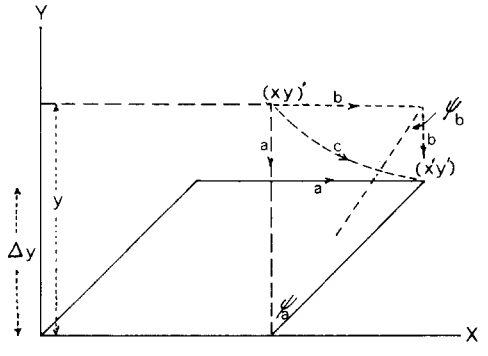

Fig. 9. Displacements and displacement paths due to simple shear and volume change. Path *a*, volume change followed by shear, *b*, shear followed by volume change and *c*, synchronous volume change and shear. ψ = angular shear strain, $\gamma = \tan \psi$.

In this section, some aspects of the strain paths in shear and thrust zones and their tips will be examined. The strain will be considered as plane strain and hence the strain path can be represented on a graph of strain ratio and orientation, θ, measured from the long axis of the strain ellipse to the shear direction. In a normal ductile shear zone, the displacements due to simple shear may be written as

$$\begin{pmatrix} x' \\ y' \end{pmatrix} = \begin{pmatrix} 1 & \gamma \\ 0 & 1 \end{pmatrix} \begin{pmatrix} x \\ y \end{pmatrix}$$

considering the deformation to be that of plane strain and hence treatable in two dimensions. If volume change (Δ) is involved, where Δ is the shortening along the y axis (Fig. 9), then the displacement gradient matrix for volume change followed by shear may be written as

$$\begin{pmatrix} 1 & \gamma_a \Delta \\ 0 & \Delta \end{pmatrix}$$

and for simple shear followed by volume change

$$\begin{pmatrix} 1 & \gamma_b \\ 0 & \Delta \end{pmatrix}.$$

The finite displacement, and hence the finite strain, depends on the order of superimposition of strains; that is, the strains are non-commutative. As shown in Fig. 9, different shear strains γ_a and γ_b are required to produce the same finite displacement for a given volume change and strain path.

As shown by Ramsay & Graham (1970) the total displacement across a shear zone may be expressed by the integral $\int_0^y \gamma_b \, dy$ where y is the distance across the zone. However, this only applies to a displacement involving shear alone or shear followed by volume change. Assuming volume change followed by shear, the same displacement may be derived from $\int_0^y \gamma_a \Delta \, dy$. Thus, for calculating displacements across a shear zone, the strain path is irrelevant. However for an understanding of the structural history, deformation mechanisms and/or chemical changes within shear zones, the sequence and intensity of strains may be important.

Similarly, assuming plane strain, a deformation gradient matrix involving longitudinal strain (shortening or elongation, $\sqrt{\lambda}$) and shear strain (γ) along the x coordinate axis (Fig. 10), but with no volume change, may be written

$$\begin{pmatrix} \sqrt{\lambda} & \dfrac{\gamma_a}{\sqrt{\lambda}} \\ 0 & \dfrac{1}{\sqrt{\lambda}} \end{pmatrix}$$

for shortening followed by shear, and

$$\begin{pmatrix} \sqrt{\lambda} & \sqrt{\lambda}\,\gamma_b \\ 0 & \dfrac{1}{\sqrt{\lambda}} \end{pmatrix}$$

assuming shear followed by shortening. As shown in Fig. 10 and discussed by Coward & Kim (1980) and Sanderson (1982), for the same finite deformation

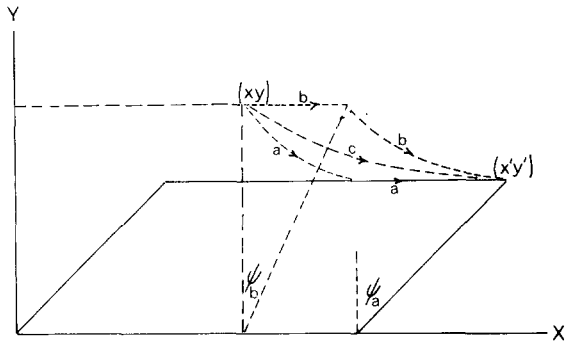

Fig. 10. Displacements and displacement paths involving shortening or elongation ($\sqrt{\lambda}$) in the x direction and simple shear. Path a, elongation followed by shear, b, shear followed by elongation, and c, synchronous elongation and shear.

$$\begin{pmatrix} \sqrt{\lambda} & \frac{\gamma_a}{\sqrt{\lambda}} \\ 0 & \frac{1}{\sqrt{\lambda}} \end{pmatrix} = \begin{pmatrix} \sqrt{\lambda} & \sqrt{\lambda}\gamma_b \\ 0 & \frac{1}{\sqrt{\lambda}} \end{pmatrix}$$

hence

$$\frac{\gamma_a}{\sqrt{\lambda}} = \sqrt{\lambda}\gamma_b$$

$$\gamma_a = \lambda\gamma_b.$$

It is these displacements which are applicable to the tips of thrust zones and to some extent to the tips of ductile shear zones. The sequence of strains, or strain path, for simple shear, plotted on a graph of strain ratio against orientation, is given in Fig. 6. Figure 11 shows three possible strain paths of simple shear with longitudinal strain: (a) is initial longitudinal strain followed by simple shear and (b) is initial simple shear followed by longitudinal strain. These are the two limiting strain paths; the general path arises by simultaneous combinations of shear strain and longitudinal strain such as Fig. 11(c) which assumes constant strain rate throughout deformation. In such a process, the longitudinal strains will increase exponentially and the shear strains, γ, will increase linearly. A detailed analysis of such a strain path was given by Ramberg (1975) and an analysis of the displacements and hence finite strain ratios and orientations was given by Coward & Kim (1981).

The strain path within the tip region of a shear zone, where the deformation does not involve simple shear alone, cannot be determined from finite strain data alone. If the strains are to be factorized, a strain path must be assumed. Some idea of the strain path may be obtained from textural studies. However, a late phase of coaxial or non-coaxial deformation may obliterate the earlier textural pattern. Thus, Christie (1960) and Riekels & Baker (1977) recorded an orthorhombic symmetry to a quartz c-axis distribution from mylonites in the Moine thrust zone of Scotland. This pattern suggests coaxial deformation was important at least during the late stages of movement in this mylonite zone.

Possibly the most powerful method of determining a strain path is to use the incremental extension history which may be deduced from fibrous overgrowths to rigid particles in the rock and the fibrous infillings to veins (Elliott 1972, Durney & Ramsay 1973, Ramsay 1981). For some of the Alpine Helvetic thrust sheets, Durney (1972) was able to show that the total strain calculated from fibrous growths in pressure shadows was the same as that derived from deformed oolites nearby. However, even if the fibres do not always record the total strain, they should give an idea of the incremental strain history which could be used in factorizing finite strain measurements.

It is emphasized, that when strain factorization is undertaken where the strain path is critical, field evidence must be used to determine the possible strain paths; these cannot be assumed, simply from the finite state.

Displacement and strains associated with lateral tips

The displacements associated with lateral tips are shown in Fig. 12 and can be written in matrix form as

$$\begin{pmatrix} 1 & \gamma_2 & \gamma_1 \\ 0 & 1 & 0 \\ 0 & 0 & 1 \end{pmatrix}$$

where γ_1 is the shear strain on the plane normal to y and γ_2 is the shear strain on the plane normal to z. Both shear strains have the same movement direction x. Combinations of these simpe shears γ_1 and γ_2 lead to the production of a simple shear strain γ_s with a shear plane oblique to that of γ_1 and γ_2 but with the same movement direction (Coward & Kim 1981, Flinn 1980). The combination gives the same result as rotating a simple shear system of

$$\begin{pmatrix} 1 & 0 & \gamma_s \\ 0 & 1 & 0 \\ 0 & 0 & 1 \end{pmatrix}$$

through an angle ϕ about the movement direction (x), giving

$$\begin{pmatrix} 1 & \gamma_s \sin\phi & \gamma_s \cos\phi \\ 0 & 1 & 0 \\ 0 & 0 & 1 \end{pmatrix}.$$

Thus, γ_1 is equivalent to $\gamma_s \cos\phi$ and γ_2 is equivalent to $\gamma_s \sin\phi$ and hence $\gamma_1/\gamma_2 = \cot\phi$. The orientation of the resultant shear plane, of γ_s, may be found from the ratio of γ_1/γ_2.

The effect of the γ_2 strain on the fabric orientation in a shear zone is shown in Fig. 13. The pole to the foliation plane, that is the $\sqrt{\lambda_1}\sqrt{\lambda_2}$ principal plane of the strain ellipsoid, will not lie on the xz plane but on a great circle at angle $\phi = \arctan \gamma_2/\gamma_1$ to the z direction. The pole to the foliation will lie at angle θ from the pole to the shear plane, where θ depends on the intensity of shear strain γ_s, and may be determined by the relationship $\tan 2\theta = 2/\gamma_s$ (Jaeger 1956), where $\gamma_s = (\gamma_1^2 + \gamma_2^2)^{1/2}$.

The finite strain trajectories, therefore, should not be straight, but arcuate in plan and spoon shaped in three

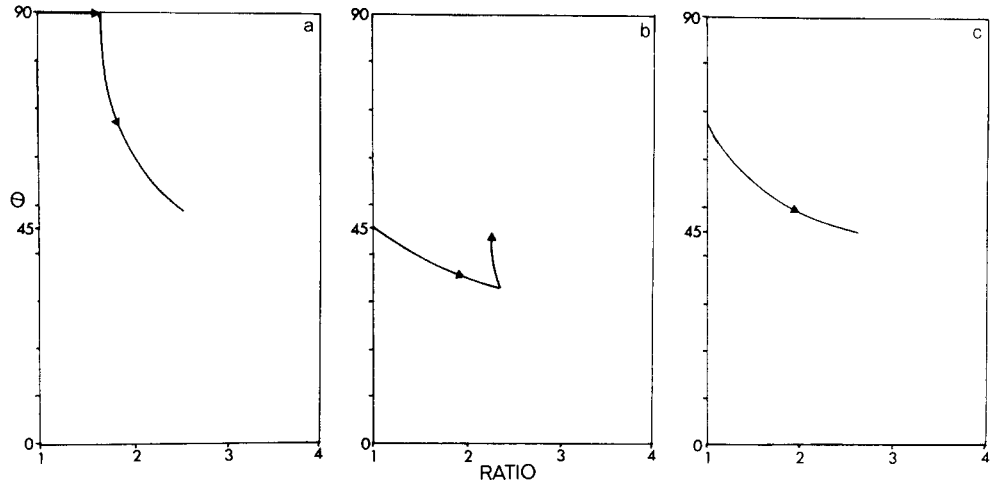

Fig. 11. Series of strain paths. (a) Layer-parallel shortening or elongation followed by shear, (b) shear followed by elongation and (c) simultaneous superimposition of shear strain and layer-parallel elongation assuming constant strain rate. These are plotted in a graph of strain ratio against θ, the angle between the long axis of the ellipse and the shear direction. Note, these paths could equally apply to combinations of simple shear and volume change. For more details of these paths and the graphs see Coward & Kim (1981).

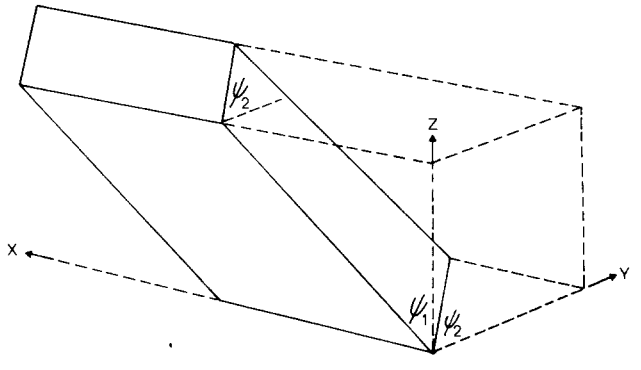

Fig. 12. The shear strain $\gamma_1 = \tan \psi_1$ related to the main layer parallel shear in a thrust system and the shear strain $\gamma_2 = \tan \psi_2$ due to differential movement of this thrust in a lateral tip, shown relative to the coordinate system x, y and z.

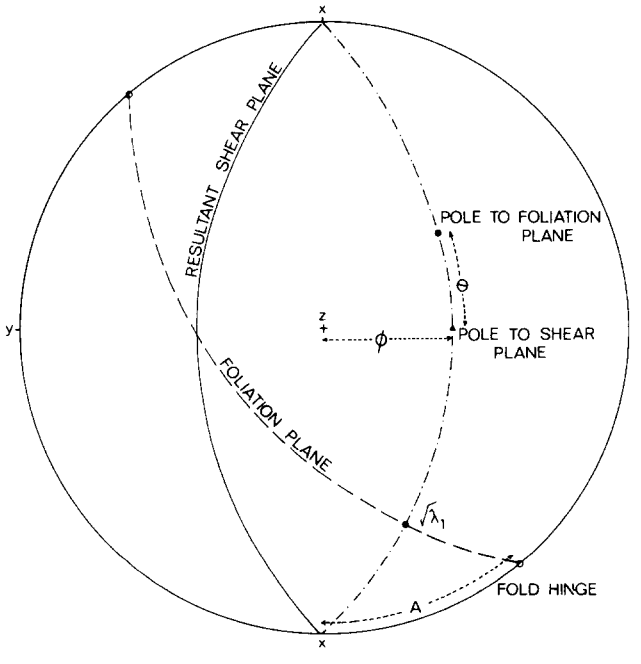

Fig. 13. The shear plane formed from a combination of the two shear strains γ_1 and γ_2, where here, γ_2 is considered to be dextral. Layering parallel to the xy plane (the main shear plane) may be buckled to produce a fold hinge at angle A, oblique to the thrust transport direction x.

dimensions; the $\sqrt{\lambda}_1$ and $\sqrt{\lambda}_2$ trajectories should be convex in the movement direction. Spoon-shaped foliation surfaces have been described in glaciers below ice falls, presumably where there was local differential movement leading to γ_2 shears (Allen *et al.* 1960, Ragan 1969). No arcuate foliation patterns have as yet been described from ductile shear zones.

As discussed earlier, this differential movement involving γ_2 leads to the production of folds oblique to the transport direction. The shear plane is a surface of no finite longitudinal strain and thus assuming simple shear γ_1 alone, when the shear is parallel to bedding or other planar fabric, no folds should be produced. However, with a component of differential movement this planar surface will be crumpled and folds produced, as shown in Fig. 13. With increase in strain intensity these fold hinges will be rotated passively toward the transport direction. Figure 14 shows how the rate of rotation depends on the ratio of γ_1/γ_2; the graph shown in Fig. 14 assumes a constant γ_1/γ_2 ratio. With only slight γ_2 strains compared to γ_1, the rate of rotation of fold axes increases markedly. With intense strain, the fold hinges will approach the transport direction but will differ from normal sheath folds (Cobbold & Quinquis 1980) in that the hinges should not be curvilinear and the folds should all face one way (Fig. 15). Thus the identification of constant facing to folds in a shear zone may be one way of identifying a differential movement component, γ_2, in a shear zone (Rattey & Sanderson 1982). As shown in Fig. 15, the facing direction of the folds indicates the γ_2 shear sense.

The finite strain ellipsoids in thrust and shear zones

The combination of the two simple shears leads to the production of a finite simple-shear zone and hence a plane-strain ellipsoid (cf. Ramsay 1980). However, if a component of layer-parallel shortening or extension along the x coordinate direction is introduced, as would

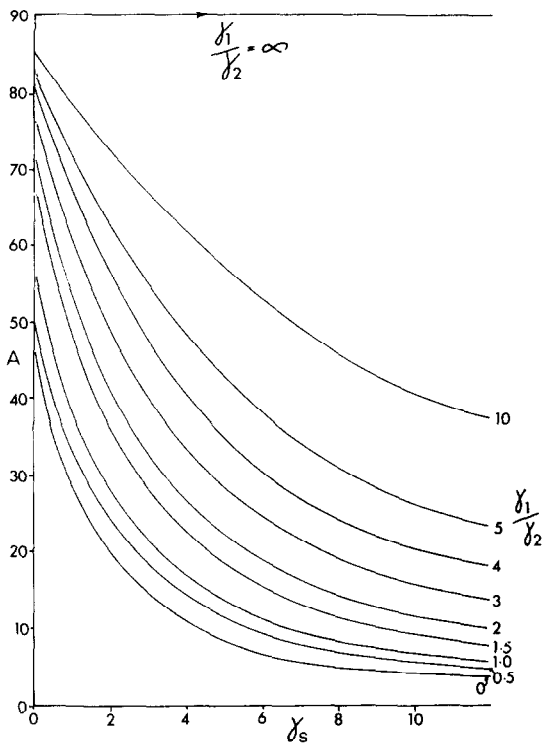

Fig. 14. The passive rotation of fold hinges and decreasing angle A to the thrust transport direction (Fig. 13), with increase in total shear strain γ_s. γ_s is produced as a result of the combination of shear strains γ_1 and γ_2. The plot shows the different rates of rotation for different but constant ratios of γ_1/γ_2.

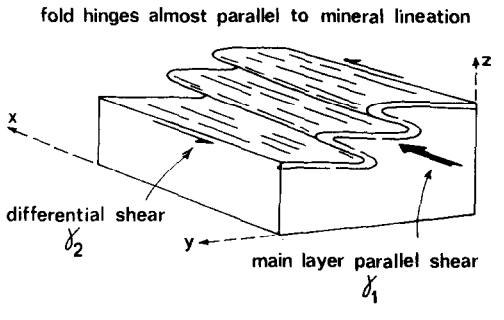

Fig. 15. Block diagram showing fold hinges rotated almost into the shear direction, and the folds verging in the same direction.

be produced near the frontal or rear tip to shear zones, there may be a wide range of finite strain ellipsoids produced. For longitudinal strain followed by shear, the displacement may be written as

$$\begin{pmatrix} \sqrt{\lambda} & \gamma_{a^1} & \gamma_{a^1}/\sqrt{\lambda} \\ 0 & 1 & 0 \\ 0 & 0 & 1/\sqrt{\lambda} \end{pmatrix}.$$

The values of the principal strains ($\sqrt{\lambda}_1$, $\sqrt{\lambda}_2$ and $\sqrt{\lambda}_3$) and their orientations may be found from the eigenvalues and eigenvectors of the tensor produced by the multiplication of the above displacement by its transpose (see Sanderson *et al.* 1980, Coward & Kim 1981 for more details). The range in ellipsoid shapes is shown in Fig. 16, for four values of $\sqrt{\lambda}$, plotted on a logarithmic Flinn-type plot (Flinn 1962). The ordinate of this plot is $A = \log_e \sqrt{\lambda}_1/\sqrt{\lambda}_2$, the abscissa is $B = \log_e \sqrt{\lambda}_2/\sqrt{\lambda}_3$ and the type of ellipsoid may be defined by its k value where $k = A/B$. For values of $\sqrt{\lambda}$ less than one, the resultant ellipsoids lie in the oblate field of the Flinn plot with $k < 1$. For values of $\sqrt{\lambda}$ greater than one, that is for layer-parallel extension or extensional flow with γ_{a^1} and γ_{a^2} strains, the resultant finite ellipsoid is in the prolate field, with $k > 1$. The dashed lines indicate strain paths formed by the superimposition of γ_{a^1} and γ_{a^2} shear strains; for a more detailed explanation see Fig. 16.

It can be seen in Fig. 16 that there is a close similarity in the shapes of individual strain paths. (They form part of a set of complex curves, constructed for the full range of ellipsoid shapes in Fig. 25.) Using these curves it is possible to factorize any finite strain represented by a point on the Flinn plot, into different components of γ_1 and γ_2, as long as a particular longitudinal strain ($\sqrt{\lambda}$) is known or assumed. Details of the process are given in the Appendix.

A displacement involving shear followed by layer-parallel shortening or elongation may be represented by the displacement matrix

$$\begin{pmatrix} \sqrt{\lambda} & \gamma_{b^2} & \gamma_{b^1}\sqrt{\lambda} \\ 0 & 1 & 0 \\ 0 & 0 & 1/\sqrt{\lambda} \end{pmatrix}.$$

The principal strains and their orientations may be found for a range of values of γ_{b^1}, γ_{b^2} and $\sqrt{\lambda}$ and plotted on a logarithmic Flinn plot as for the previous case. The plots have the same form as those produced by shortening predating shear and the shape of the curves given by the different increases in increments of γ_{b^1} and γ_{b^2} are the same. However, the values of these γ_{b^1} and γ_{b^2} curves are different from those produced by shortening before shear, again showing that knowledge or an assumption of the sequence of strain is important when considering a finite strain and its strain path.

Using Fig. 16, values for γ_{b^1} and γ_{b^2} may be obtained from

$$\gamma_{b^1} = \frac{\gamma_{a^1}}{\lambda}$$

and

$$\gamma_{b^2} = \frac{\gamma_{a^2}}{\sqrt{\lambda}}.$$

The strain paths followed by the shape of the finite strain ellipsoid on the Flinn plot for shear pre-dating shortening are shown in Fig. 17 for various values of γ_{b^1} and γ_{b^2}. These curves have a very different form from those of shortening pre-dating shear (compare Figs. 16 & 17).

Some idea of the range in orientations of the finite strain ellipsoids is given on the stereographic plot in Fig. 18. With increase in layer parallel shortening the $\sqrt{\lambda}_1$ axis lies closer to the z coordinate axis but is deflected from the xz plane by addition of γ_2 shear strains. This deflection is more pronounced for the less intense values of shortening strain. The rate of apparent rotation of the

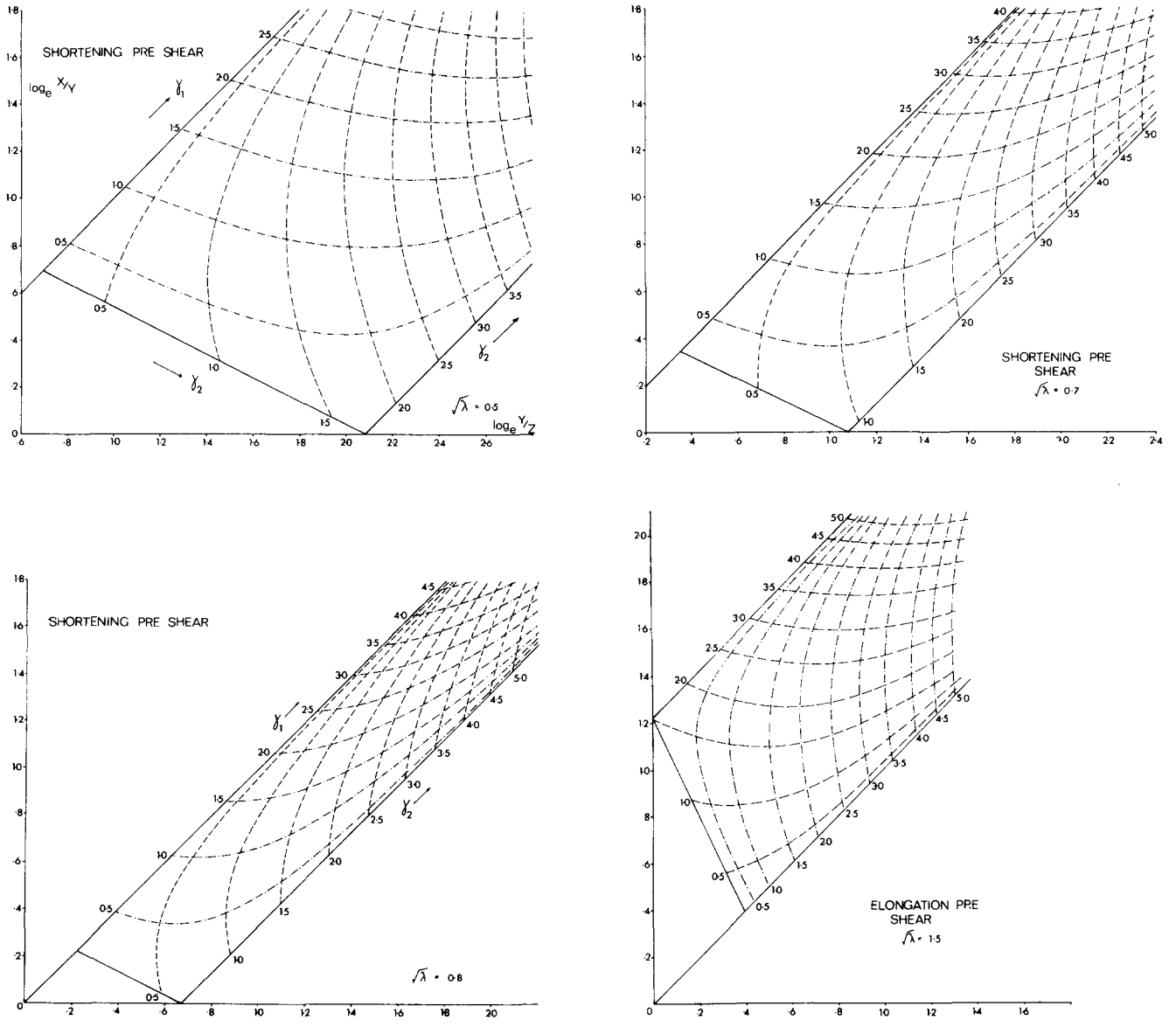

Fig. 16. Logarithmic Flinn plots, ordinate $A = \log_e \sqrt{\lambda}_1/\sqrt{\lambda}_2$, abscissa $B = \log_e \sqrt{\lambda}_2/\sqrt{\lambda}_3$ (or $\log_e X/Y$ and $\log_e Y/Z$, respectively) for strains involving longitudinal strain followed by shear. Assuming strain sequences involving longitudinal strain and shear γ_1, the strain path follows the $k = 1$ line (where $k = A/B$). With an addition of γ_2 shear strains, the strain path moves into the oblate field for paths involving layer-parallel shortening but moves into the prolate field for paths involving layer-parallel elongation. The dot–dash lines can be considered as strain paths for increasing γ_2 (constant γ_1) and the dashed lines strain paths for increase in γ_1 (constant γ_2). Together these lines form a grid on the Flinn plot which give the position of any strain involving $\sqrt{\lambda}$, γ_1 and γ_2. Hence the dash–dot lines represent contours of equal value of γ_1, the dashed lines, contours of equal value of γ_2. Plots are given for four values of longitudinal strain ($\sqrt{\lambda}$). See text for discussion. (Similar plots for shear preceding shortening available on request.)

$\sqrt{\lambda}_1$ axis towards the x coordinate direction for an increase in shear strain γ_1 and/or γ_2 is more rapid if shortening pre-dates shear rather than if shear pre-dates shortening (compare the $\sqrt{\lambda}_1$ directions for Figs. 18c & d). Stereographic plots (b) and (d) show the strain paths produced by shortening followed by shear. Strain paths given by shear followed by shortening are given in Fig. 19 for two strain sequences $\gamma_1 = \gamma_2 = 0.5$ and $\gamma_1 = 0.5$, $\gamma_2 = 2.0$.

For shear with layer-parallel elongation the $\sqrt{\lambda}_1$ direction lies close to the x coordinate axis for most values of γ_1 and γ_2. In many shear zones, therefore, which involve extensional flow, it may be difficult to identify variations in orientation of the finite strain ellipsoids due to shear strain γ_2.

Finite strain ellipsoids which plot in the oblate or prolate fields may also be produced by combinations of simple shear and volume change (Sanderson 1976). The displacement may be written as

$$\begin{pmatrix} 1 & \gamma_{a^2} & \gamma_{a^1}\Delta \\ 0 & 1 & 0 \\ 0 & 0 & \Delta \end{pmatrix}$$

where volume change pre-dates shear and Δ is the

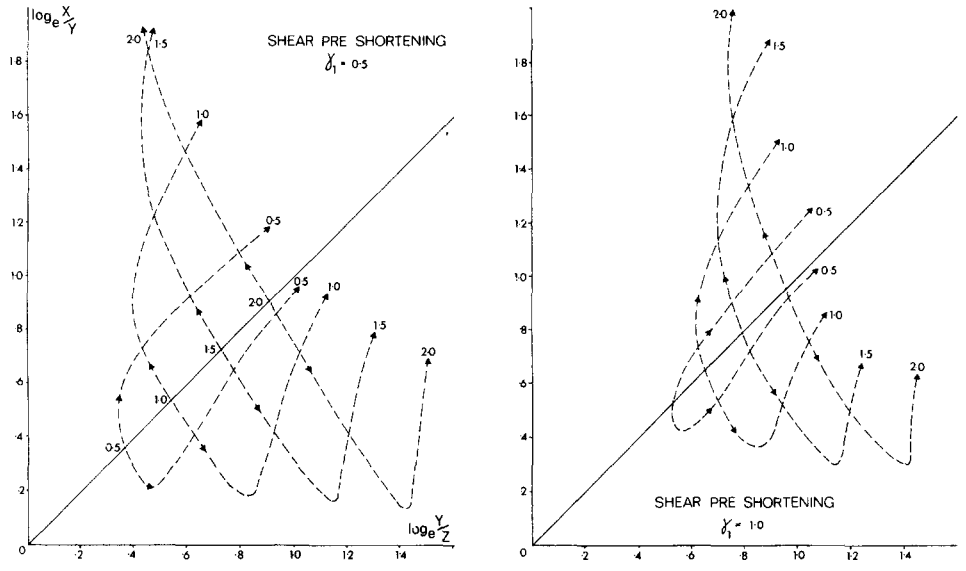

Fig. 17. Strain paths on logarithmic Flinn plots for sequences of strain involving shear (γ_b) followed by longitudinal strain, compressive on the oblate side of the $k = 1$ line, extensional on the prolate side. The paths are plotted for four different values of γ_2, from 0.5 to 2.0, for two values of γ_1. With only γ_1 and γ_2, the finite strain lies on the $k = 1$ line. With increase in longitudinal strain, the strain path at first moves away from the $k = 1$ line but then follows a complex curve to become slightly steeper than the $k = 1$ line.

shortening along the z axis due to volume change. If shear precedes volume change the displacement is

$$\begin{pmatrix} 1 & \gamma_{b^2} & \gamma_{b^1} \\ 0 & 1 & 0 \\ 0 & 0 & \Delta \end{pmatrix}.$$

The values of the principal strains may be found as described previously. The finite strain ratios for some combinations of Δ, γ_1 and γ_2 are given in Fig. 20. As with the combinations of shear and longitudinal strain, the shape of the finite strain ellipsoid depends on the strain sequence (compare a and b). The strain paths given by volume change followed by shear are given in Fig. 20. Volume loss with a shear γ_1 gives a path slightly in the oblate field, parallel to the $k = 1$ line. This path intersects the abscissa of the Flinn plot at a value $V = \log_e (1/\Delta)$. Volume loss with a γ_2 shear strain gives a similar straight-line plot, parallel to $k = 1$, but in the prolate field (cf. Sanderson 1976) and this line intersects the ordinate of the Flinn plot at $2V$. For combinations of γ_1 and γ_2 in Fig. 20 the paths are more complex.

DISCUSSION AND CONCLUSIONS

The strains in thrust zones pose less compatibility problems than strains within deeper level ductile shears. The fault planes act as major discontinuities in strain and thus it is only the thrust sheet above the thrust plane that need be affected by thrust tips and the associated shortening strains and γ_2 shear strains due to the differential movement. Sometimes the thrust sheets are thick and the regional development of folds and cleavage may be related to the tips and the branching of only a few major thrusts. Elsewhere the thrust sheets may be thin, as in the Eriboll region of the Moine thrust zone (Fig. 2), where bedding planes in some of the Cambrian quartzites have acted as individual decoupling planes, causing rapid variation in strain. As, in general, low-level thrusts are later than higher thrusts (cf. Dahlstrom 1970), the higher-level thrust sheets may suffer several phases of straining due to deformation on successively lower thrust planes. Folds developed on one sheet may be refolded by structures developed on a lower sheet. Similarly, the cleavage development may be progressive, formed by layer-parallel shortening or shear strains on several different thrust sheets. If during the development of different thrust sheets, the thrusts spread from different source areas, lateral tip strains with, say, a dextral γ_2 shear component might interfere with frontal-tip strains, or lateral-tip strains with a sinistral γ_2 component. This may lead to complex fold interference patterns (Fig. 21). Thus, during the development of a thrust zone several generations of cleavage and folds may form locally, all related to the same thrust movement, but generated at the tips of different thrust sheets.

An analysis of the tip strains should give an indication of the rate at which fault displacements die out. Elliott (1976) noted a relationship between the strike length (l) of a thrust on a map and its displacement u

$$u = fl$$

where f is about 0.07. As the maximum displacement is generally at the centre of the thrust, at the bisector of the straight line joining the two ends of the thrust on a map (the 'bow and arrow' rule of thumb, Elliott 1976), the average γ_2 shear strain should be $7/50 = 0.14$. Thus if the shear at the lateral tip were to decrease gradually, the shear strain would probably not be detected. However, in the Assynt and Eriboll areas of the main thrust zone (Fig. 3) the shear strain is intense and the displacement

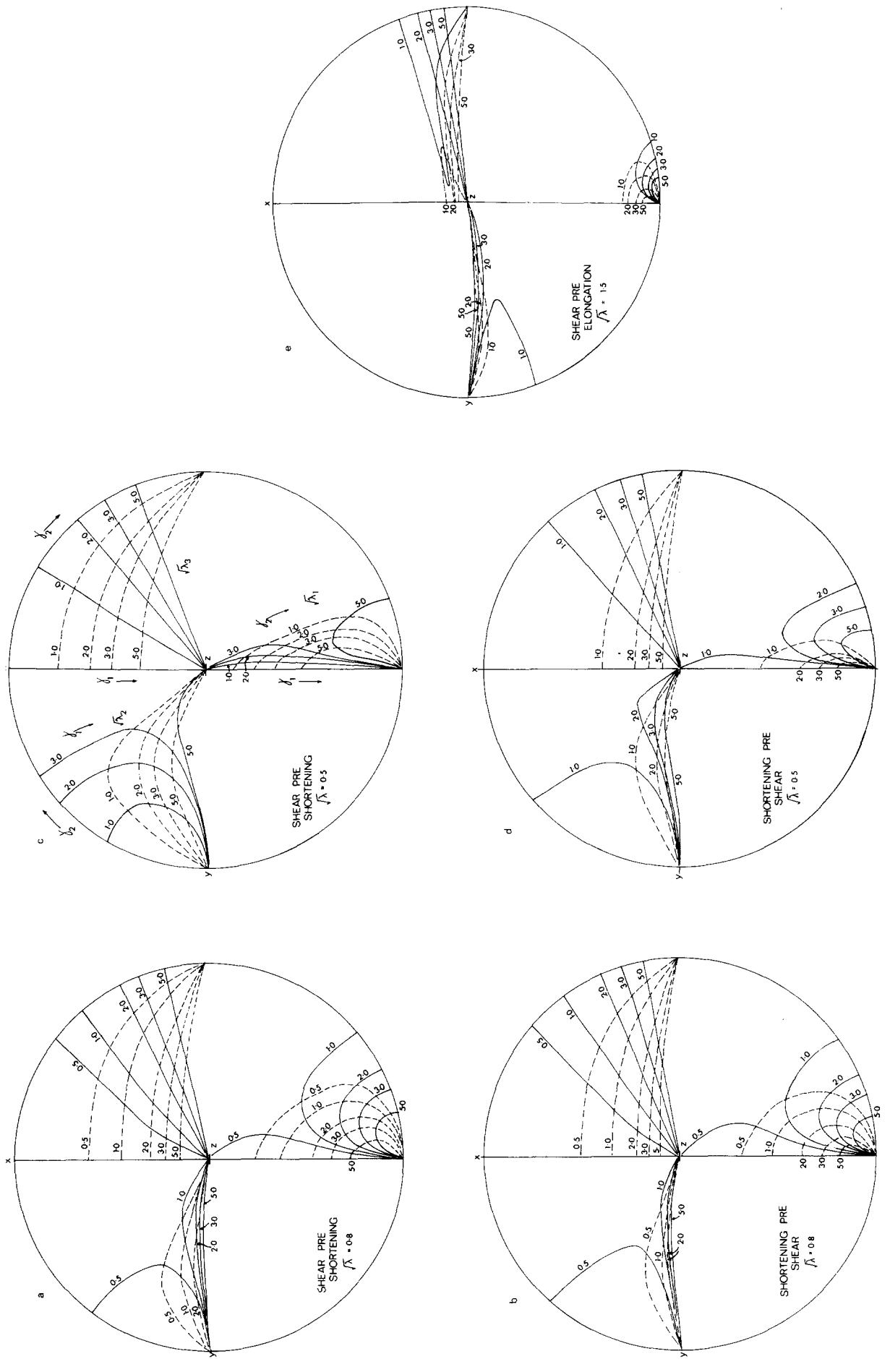

Fig. 18. Stereographic plots showing the range in orientations of the principal strain axes for strain sequences involving $\sqrt{\lambda}$, γ_1 and γ_2. The dashed lines are contours of equal γ_1 strains, the solid lines are contours of equal γ_2 strain. (a) and (b) show plots for longitudinal strains of $\sqrt{\lambda} = 0.8$ but with shear pre- and post-longitudinal strain; the contours for γ_1 and γ_2 have the same form but the values are different. In (b) the contours are equivalent to the paths made by the principal strain axes with increase in shear strain. (c) and (d) as (a) and (b) but with $\sqrt{\lambda} = 0.5$; (e) for shear pre-elongation, $\sqrt{\lambda} = 1.5$.

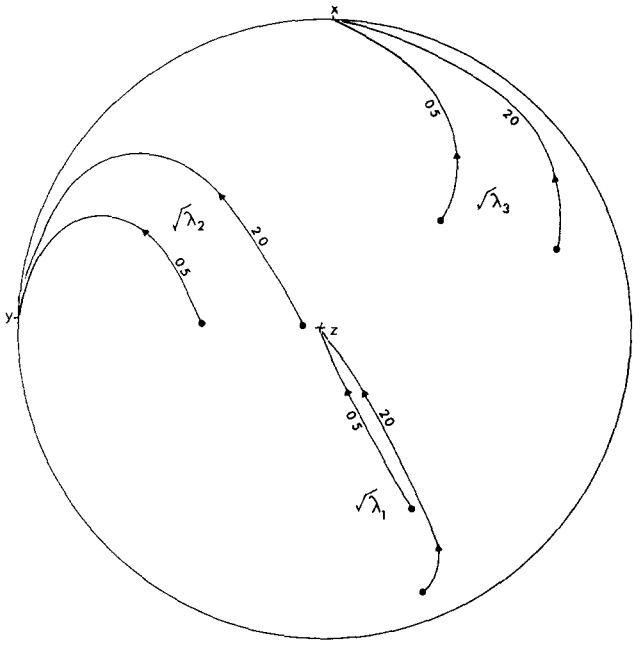

Fig. 19. Stereographic plot showing the paths made by the axes of finite strains formed by the addition of longitudinal strains to shear strains of $\gamma_1 = 0.5$, $\gamma_2 = 0.5$ and $\gamma_1 = 0.5$, $\gamma_2 = 2.0$, numbered on the figure.

profile probably represented by Fig. 22(b). This would suggest that there were zones where the fault could move easily, separated by a zone of intense tip strain from a region where forward displacement was less. Strain profiles at the frontal and lateral tips to thrust zones should therefore give us some idea of the variation in fault mechanisms and possibly an indication of the energy involved in fault movement (cf. Elliott 1976). The more intense strains as developed in Fig. 22(b) are generally associated with the development of new faults; that is they are associated with branch lines.

For a factorization of tip strains into different strain components, a strain path should be known or assumed. Sanderson (1982) has argued that longitudinal strain followed by shear is the most useful sequence to assume as generally at frontal tips, a longitudinal strain will pre-date or be synchronous with the main γ_1 shear strain. In a thrust zone, however, longitudinal strains may develop at the tips of lower thrusts and hence post date any shear strains in the higher thrust sheets. In general, the strain path will be complex and a solution is

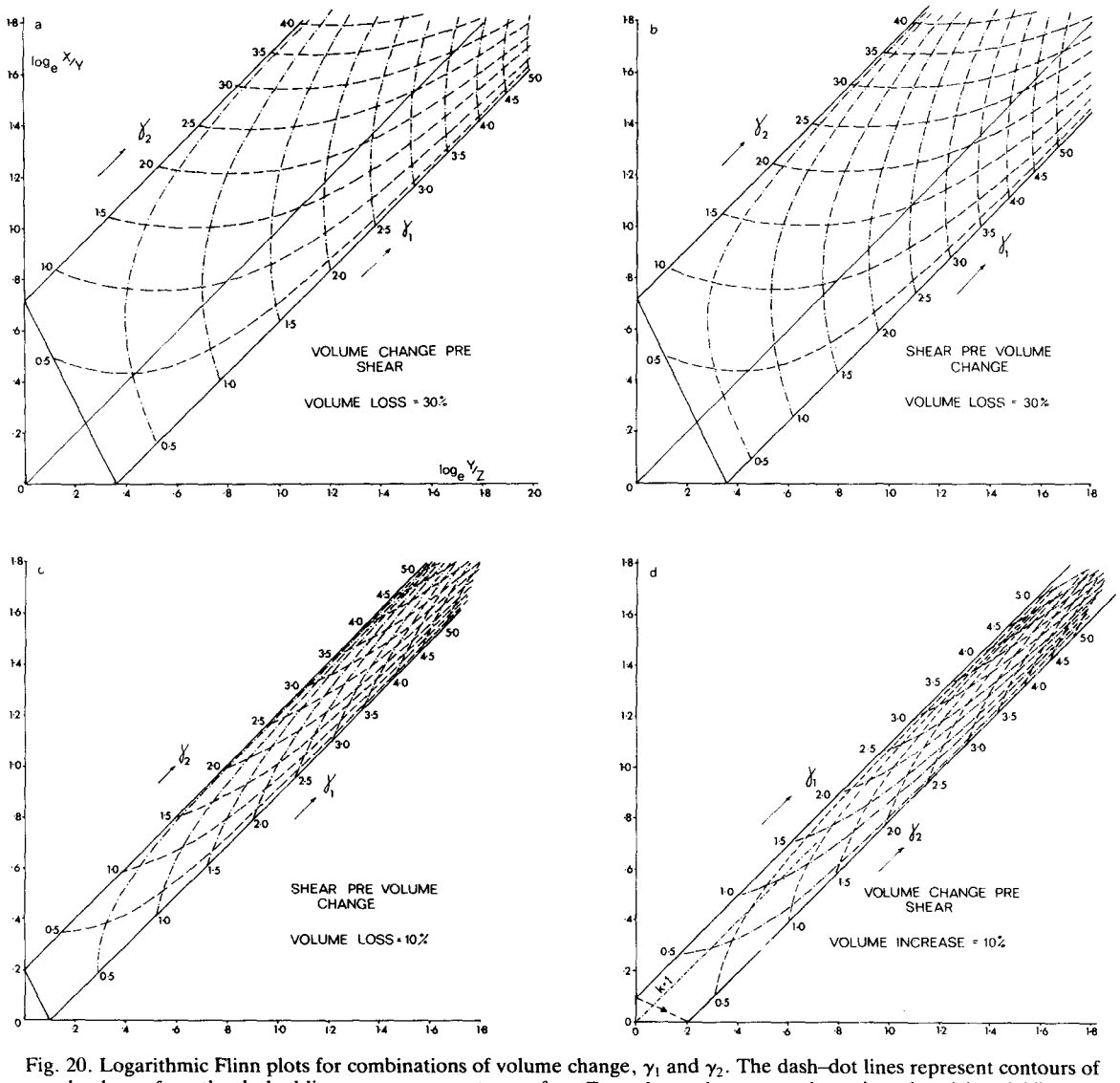

Fig. 20. Logarithmic Flinn plots for combinations of volume change, γ_1 and γ_2. The dash–dot lines represent contours of equal values of γ_1, the dashed lines represent contours of γ_2. For volume change pre-shear, i.e. plots (a) and (d) these contours also represent strain paths for increase in shear strain. See Figs. 17(c) & (d) for more explanation.

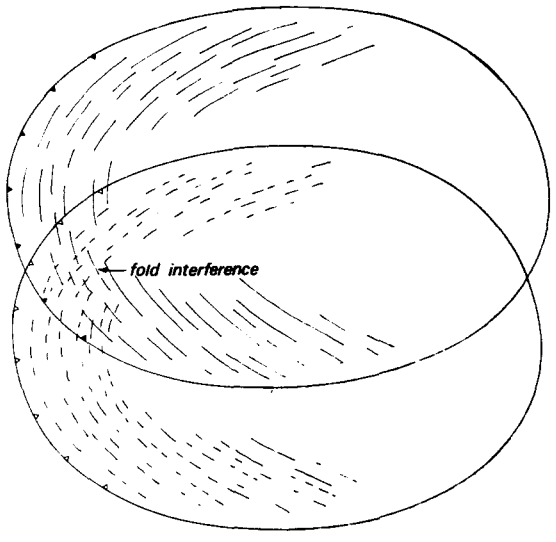

Fig. 21. Fold interference may be produced where tip strains for one thrust movement interfere with tip strains from another, even though the deformation may be part of the same thrust sequence.

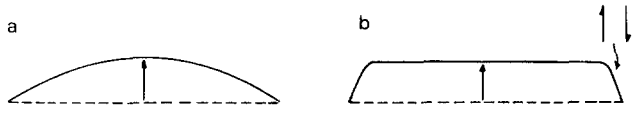

Fig. 22. (a) The bow and arrow model for thrust displacement, after Elliott (1976). The solid line bounds the displaced area of a thrust, the displacement direction is shown by the arrow, the dashed line the original thrust branch line. With this model the displacement dies out smoothly to the lateral thrust tips. (b) The variation in displacement suggested by the locally intense γ_2 strains in the north Eriboll and north Assynt areas (cf. Fischer & Coward 1982, Coward & Kim 1981 and text for discussion).

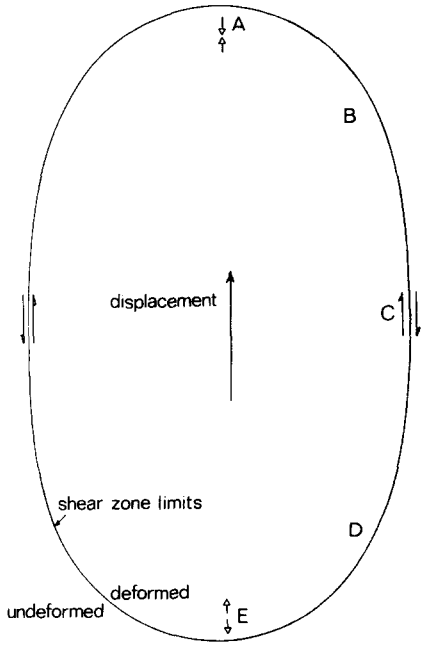

Fig. 23. Variations in k value within a shear zone, near the fault tips. At A, C and E the strains are of $k = 1$. At B they tend to be more oblate. At D they tend to be more prolate. See text for details.

only possible if the incremental strain history is known from fibre growths (cf. Ramsay 1981).

It has long been known that thrusts die out into folds along strike and often cut through folds at their frontal tips. Heim (1921) described this relationship between folds and thrusts in the Alps, and Willis (1893) produced models of faults cutting through overturned fold limbs simulating Appalachian structures. At the lateral tips to thrusts these folds will be oblique to the thrust transport direction and, with increase in shear strain, they will rotate towards the transport direction. Thus, in many mylonite zones and also the higher-grade metamorphic parts to orogenic belts, many of the large fold systems have axes nearly parallel to the extension direction in the rock and often face in one dominant direction. It may be possible to map out zones of dominant facing or vergence direction and from this map out zones of different γ_2 shears. Downing & Coward (1981) applied this concept on a large scale to the high-grade rocks of the early Phanerozoic Damaran orogenic belt in Namibia. They mapped out regions where the large and small scale folds have sheath-like geometry and regions where the folds have constant vergence, yet lie close to the maximum elongation direction. The rocks are deformed by a large low-angle shear zone, and Downing & Coward (1981) show that there are large zones within this shear where the folds have constant vergence, suggesting a large component of differential sinistral movement. Rattey & Sanderson (1982) have described similar patterns of thrust movement using the change in trend of fold axes in SW England. Ridley (1982) has used fold hinge trends to map out zones of differential movement in a high grade shear zone in the Aegean. If using this technique, care must be taken to separate folds caused by a buckling component from those formed by the accretion of lateral ramps (see Fig. 5) and from similar-type folds formed by flow over an irregular surface or some other anisotropy in the rock (cf. Hudleston 1977, Cobbold & Quinquis 1980, Talbot 1981).

The rear tips to extensional faults and some of the tip regions of ductile shear zones may show the development of closely-spaced normal faults or normal ductile shears, which form an extensional crenulation cleavage (Platt & Vissers 1980). The intersection of the shear bands with the main shear foliation should be normal to the transport direction, though with components of a γ_2 lateral tip strain, the shear bands may be more oblique to the transport direction.

The shape of the strain ellipsoid may vary throughout a thrust or shear zone as a result of the addition of differential movement and lateral tip strains γ_2 to the main shear strain γ_1, and volume change across the zone and/or layer-parallel longitudinal strains. Within the tips to a slipped region such as that shown in Fig. 23, at points A and E the rocks have suffered longitudinal strain plus the main shear strain γ_1 and hence produce a $k = 1$ finite strain ellipsoid. At C the rocks suffer a finite simple shear strain γ_s as a result of the combination of the two shears γ_1 and γ_2. The finite strain here is also of $k = 1$. At B however, the rocks suffer layer-parallel shortening as well as shear γ_1 and γ_2 and the strains may be nearly

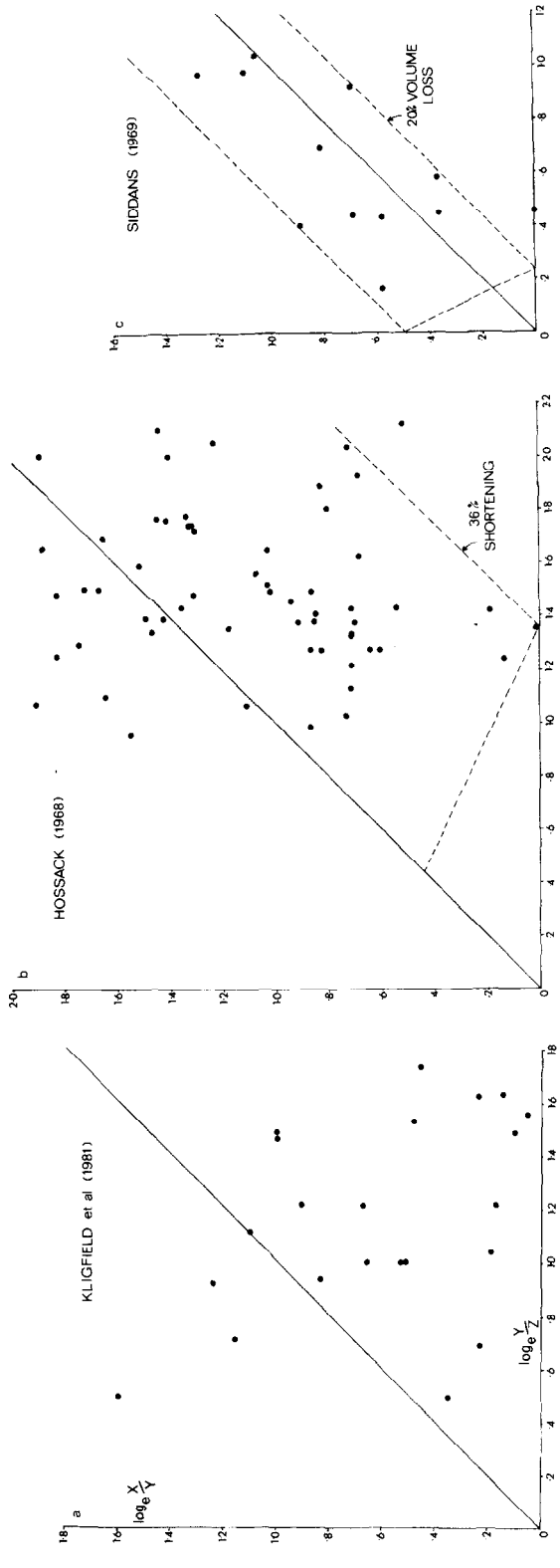

Fig. 24. Logarithmic Flinn plots of strain data from Kligfield *et al.* (1981), Hossack (1968) and Siddans (1979). See text for discussion. Axes as for Figs. 16 and 21.

oblate, while at D, where there has been some layer-parallel extension, the finite strain will be prolate.

These combinations of displacements may be one way to explain some of the variations in strain ellipsoid shapes in many thrusts, shears and major orogenic belts. Kligfield *et al.* (1981) recorded a wide range of ellipsoid shapes from thrust sheets in the Appenines (Fig. 24a) and Hossack (1968) a range from $k = 0$ to $k > 3$ from the Bygdin conglomerates in the Valdres nappe beneath the Jotun nappe in the Caledonian thrust zone of Norway (Fig. 24b). Hossack (1968) suggested that this variation in k value may be due to constriction or extension of the Valdres nappe, possibly due to movement over an irregular surface. An alternative suggestion is that the variation in k value may be produced by a combination of longitudinal and shear strains as described above, without any change in length of the thrust sheet normal to the transport direction. Variations in k value of the finite strain ellipsoid have been reported from the Funzie conglomerates of Shetland (Flinn 1956) and from Caledonian thrust sheets of northern Norway (Chapman *et al.* 1979). Strains of $k \neq 1$ appear to be the rule rather than the exception in thrust sheets.

Note that this argument for no change in length normal to the transport direction need not always apply in thrust sheets, even when maintaining no change in overall length of the thrust belt parallel to strike. Butler (1982) pointed out that above thrust culminations, rocks may be stretched over a locally tectonically thickened mass. This could lead to extensional strains normal to the transport direction, with elongation of up to 20%. This would cause the finite strain ellipsoids to lie in the oblate field on the Flinn plot, where no differential movement (γ_2 strain) is involved.

Where volume change is involved in the deformation, finite strain ellipsoids which lie off the $k = 1$ line on the Flinn plot may be formed at the lateral tips to shear zones; prolate strains for example are not confined to the region affected by lateral and rear tips. A possible example of a strain distribution involving shear and volume change is given by the data of Siddans (1979) from the Glarus thrust sheet (Fig. 24c). These data are taken from strained green spots in mudstones near the top of the Permian Verrucano overlying the Glarus thrust. The flattening planes dip gently south, and the extension direction is orientated north–south, presumably close to the shear direction. All the data points lie within the boundary field for 20% volume loss, a reasonable figure for volume change and one not so different from that estimated by Graham (1978) for similar green spots in Permian shales in the southern French Alps. However, there may be other explanations for the $k \neq 1$ ellipsoids. From the sections of Siddans (1979, based partly on sections of Trumpy 1969 and Schmid 1975) and the orientations of the ellipsoids relative to the Glarus thrust plane, there may have been extensional flow involved in the nappe deformation. Siddans (1979) estimated a bulk extension of 14% along part of the Glarus thrust sheet. However, as Siddans pointed out, the deformation dies out upwards, so that the overlying Jurassic and Cretaceous strata are generally undeformed, apart from the presence of large and often oblique folds (Pfiffner 1981). These folds have axes trending between E–W and N–S, sometimes close to the shear direction. Often these folds are associated with lateral and oblique ramps (Pfiffner 1981) suggesting some local shortening or compressive flow. Thus, there are compatibility problems in accommodating the strain upwards assuming extensional flow in the Verrucano. There are no such accommodation problems if the deformation is considered to involve volume change in the Verrucano and shear strain γ_1 and γ_2 throughout the Glarus thrust; the variation in the γ_2 shear could help cause some of the oblique folds and thrust ramps in the Jurassic and Cretaceous limestones.

Acknowledgements—The authors are grateful for comments both by colleagues at Leeds and the referees, which greatly improved the manuscript. This work is part of N.E.R.C. Grant 4100. G. Potts received a N.E.R.C. research studentship.

REFERENCES

Allen, C. R., Kamb, W. B., Meier, M. F. & Sharp, R. P. 1960. Structures of the lower Blue Glacier, Washington. *J. Geol.* **68**, 601–625.

Barber, A. J., Beach, A., Park, R. G., Tarney, J. & Stewart, A. D. 1978. *The Lewisian and Torridonian rocks of North-West Scotland.* Geol. Assoc. Guide, No. 21.

Berthé, D., Choukroune, P. & Jegouzo, P. 1979. Orthogneiss, mylonite and non-coaxial deformation of granites: the example of the South American shear zone. *J. Struct. Geol.* **1**, 31–42.

Butler, R. 1982. A structural analysis of the Moine Thrust Zone between Loch Eriboll and Foinaven, N.W. Scotland. *J. Struct. Geol.* **4**, 19–29.

Chapman, T. J., Milton, N. J. & Williams, G. D. 1979. Shape fabric variations in deformed conglomerates at the base of the Laksefjord Nappe, North Norway. *J. geol. Soc. Lond.* **136**, 683–691.

Christie, J. M. 1960. Mylonitic rocks of the Moine thrust zone in the Assynt region, north-west Scotland. *Trans. Edinb. Geol. Soc.* **18**, 79–93.

Cobbold, P. R., Cosgrove, J. W. & Summers, J. M. 1971. Development of internal structures in deformed anisotropic rocks. *Tectonophysics* **12**, 23–53.

Cobbold, P. R. & Quinquis, H. 1980. Development of sheath folds in shear regimes. *J. Struct. Geol.* **2**, 119–126.

Cooper, M., Garton, M. & Hossack, J. R. in press. Balanced sections and the origin of the Henaux Basse Normandie duplex, Boulonnais. *J. Struct. Geol.* **5**, 139–152.

Coward, M. P. 1976. Strain within ductile shear zones. *Tectonophysics* **34**, 181–197.

Coward, M. P. 1982. Surge zones in the Moine thrust zone of N.W. Scotland. *J. Struct. Geol.* **4**, 247–256.

Coward, M. P. & Kim, J. H. 1981. Strain within thrust sheets. In: *Thrust and Nappe Tectonics* (edited by McClay, K. R. & Price, N. J.). *Spec. Publs Geol. Soc. Lond.* **9**, 275–292.

Dahlstrom, C. D. A. 1970. Structural geology of the eastern margin of the Canadian Rocky Mountains. *Bull. Can. Petrol. Geol.* **18**, 332–406.

Douglas, R. J. W. 1958. Mount head map-area, Alberta. *Geol. Surv. Can. Mem.* **291**.

Downing, K. & Coward, M. P. 1981. The Okahandja lineament and its significance in Damaran tectonics of Namibia. *Geol. Rdsch.* **70**, 927–1000.

Durney, D. W. 1972. Deformation history of the Western Helvetic Nappes, Valais, Switzerland. Ph.D. thesis, London University (unpubl.).

Durney, D. W. & Ramsay, J. G. 1973. Incremental strains measured by systematic crystal growths. In: *Gravity and Tectonics* (edited by De Jong, K. H. & Scholten, R.). Wiley, New York, 67–96.

Elliott, D. 1972. Deformation paths in structural geology. *Bull. geol. Soc. Am.* **83**, 2621–2635.
Elliott, D. 1976. The energy balance and deformation mechanisms of thrust sheets. *Phil. Trans. R. Soc. London* **283**, 289–312.
Fischer, M. W. & Coward, M. P. 1982. Strain within thrust sheets: the Heilam sheet of N.W. Scotland. *Tectonophysics* **88**, 291–312.
Flinn, D. 1956. On the deformation of the Funzie conglomerates, Fetlar, Shetland. *J. Geol.* **64**, 480–505.
Flinn, D. 1962. On folding during three-dimensional progressive deformation. *Q. Jl geol. Soc. Lond.* **118**, 385–433.
Flinn, D. 1980. The deformation matrix and the deformation ellipsoid. *J. Struct. Geol.* **1**, 299–307.
Graham, R. H. 1978. Quantitative deformation studies in the Permian Rocks of the Alpes Maritimes. *Goguel Symposium, B.R.G.M.* 220–230.
Harris, L. D. & Milici, R. C. 1977. Characteristics of thin-skinned style of deformation in the southern Appalachians, and potential hydrocarbon traps. *Prof. Pap. U.S. geol. Surv.* **1018**.
Heim, A. 1921. *Geologie der Schweiz II. Die Schwizer Alpen.* Tauchnitz, Leipzig.
Hossack, J. R. 1968. Pebble deformation and thrusting in the Bygdin area (South Norway). *Tectonophysics* **5**, 315–339.
Hudleston, P. J. 1977. Similar folds, recumbent folds and gravity tectonics in ice and rocks. *J. Geol.* **85**, 113–122.
Jaeger, J. C. 1956. *Elasticity, Fracture and Flow.* Methuen, London.
Kligfield, R., Carmignani, L. & Owens, W. H. 1981. Strain analysis of a Northern Apennine shear zone using deformed marble breccias. *J. Struct. Geol.* **3**, 421–436.
McClay, K. R. & Coward, M. P. 1981. The Moine thrust zone: an overview. In: *Thrust and Nappe Tectonics* (edited by McClay, K. R. & Price, N. J.). *Spec. Publs geol. Soc. Lond.* **9**, 241–260.
Nadai, A. 1963. *Theory of Flow and Fracture of Solids, Vol. II.* McGraw-Hill, New York.
Peach, B. N., Horne, J., Gunn, W., Clough, C. T. & Hinxman, L. W. 1907. *The Geological Structure of the North West Highlands of Scotland.* Mem. Geol. Surv. U.K.
Pfiffner, O. A. 1981. Fold and thrust tectonics in the Helvetic Nappes (E. Switzerland). In: *Thrust and Nappe Tectonics* (edited by McClay, K. R. & Price, N. J.). *Spec. Publs geol. Soc. Lond.* **9**, 319–327.
Platt, J. P. & Vissers, R. L. M. 1980. Extensional structures in anisotropic rocks. *J. Struct. Geol.* **2**, 397–410.
Ponce de Leon, M. I. & Choukroune, P. 1980. Shear zones in the Iberian Arc. *J. Struct. Geol.* **2**, 63–68.
Ragan, D. M. 1969. Structure at the base of an ice fall. *J. Geol.* **77**, 647–667.
Ramberg, H. 1975. Particle paths, displacement and progressive strain applicable to rocks. *Tectonophysics* **28**, 1–37.
Ramsay, J. G. 1967. *Folding and Fracturing of Rocks.* McGraw-Hill, New York.
Ramsay, J. G. 1980. Shear zone geometry: a review. *J. Struct. Geol.* **2**, 83–99.
Ramsay, J. G. 1981. Tectonics of the Helvetic Nappes. In: *Thrust and Nappe Tectonics* (edited by McClay, K. R. & Price, N.J.). *Spec. Publs geol. Soc. Lond.* **9**, 293–309.
Ramsay, J. G. & Graham, R. H. 1970. Strain variations in shear belts. *Can. J. Earth Sci.* **7**, 786–813.
Rattey, P. R. & Sanderson, D. J. 1982. Patterns of folding within nappes and thrust sheets: examples from the Variscan of Southwest England. *Tectonophysics* **88**, 247–267.
Rich, J. L. 1934. Mechanics of low-angle overthrust faulting as illustrated by the Cumberland thrust block, Virginia, Kentucky, Tennessee. *Bull. Am. Ass. Petrol. Geol.* **18**, 1584–1596.
Ridley, J. 1982. Arcuate lineation trends in a deep level, ductile thrust belt, Syros, Greece. *Tectonophysics* **88**, 347–360.
Riekels, L. M. & Baker, D. W. 1977. The origin of the double maximum pattern of optic axes in quartzitic mylonites. *J. Geol.* **85**, 1–14.
Sanderson, D. J. 1976. The superposition of compaction and plane strain. *Tectonophysics* **30**, 35–54.
Sanderson, D. J. 1982. Models of strain variation in nappes and thrust sheets: a review. *Tectonophysics* **88**, 201–233.
Sanderson, D. J., Andrews, J. R., Phillips, W. E. A. & Hutton, D. H. W. 1980. Deformation studies in the Irish Caledonides. *J. geol. Soc. Lond.* **137**, 289–302.
Schmid, S. M. 1975. The Glarus overthrust: field evidence and mechanical model. *Eclog. geol. Helv.* **68**, 247–280.
Siddans, A. W. B. 1979. Deformation, metamorphism and texture development in Permian mudstones of the Glarus Alps. *Eclog. geol. Helv.* **72**, 601–621.
Talbot, C. J. 1981. Sliding and other deformation mechanisms in a glacier of salt. In: *Thrust and Nappe Tectonics* (edited by McClay, K. R. & Price, N. J.). *Spec. Publs geol. Soc. Lond.* **9**, 173–183.
Trumpy, R. 1969. Die helvetischen Decken der Ostschweiz: Versuch einer palinspastischen Korrelation und Ansatze zu einer kinematischen Analyse. *Eclog. geol. Helv.* **62**, 105–142.
White, S. 1980. Large strain deformation; report on a Tectonic Studies Group discussion meeting held at Imperial College, London, 14 November, 1979. *J. Struct. Geol.* **1**, 333–339.
Willis, B. 1893. The mechanics of Appalachian structure. *U.S. Geol. Survey, 13th Ann. Rept.* Pt. 2, 211–281.

APPENDIX

The factorization of strains on the Flinn plot

The contours for γ_1 and γ_2 shear strains on the Flinn plots (Fig. 16) form part of a family of curves, irrespective of the amount of layer-parallel longitudinal strain or the sequence of strains. These curves are shown in Fig. 25. Thus using these curves it is possible to factorize graphically the finite strains on the Flinn plot as long as the longitudinal strain is known. To put figures on the curves a strain sequence must be assumed.

The procedure is shown in Fig. 26. Firstly assume a specific $\sqrt{\lambda}$ value. This allows the boundaries to be drawn to the strain field on the Flinn plot (Fig. 26). Thus the contour for γ_2, $\gamma_1 = 0$ touches the abscissa of the Flinn plot at $P = 3 \log_n \sqrt{\lambda}$. Construct line PQ parallel to the $k = 1$ line. Use the curves in Fig. 25(b), the contours of equal γ_1 strain, to find point a on the $k = 1$ line, superimposing line PQ on the construction with that on the graph. The coordinates of point a are $\frac{1}{2}$ log Ratio where Ratio is the result of the superimposition of γ_1 and $\sqrt{\lambda}$. Thus as the Ratio is known and $\sqrt{\lambda}$ is assumed, γ_1 may be found using the normal two-dimensional strain factorization curves given by Fischer & Coward (1982), assuming shortening pre- or post-shear. Using the curves in Fig. 25(a) find point f on line PQ, superimposing the $k = 1$ line on the construction and Fig. 25(a). Point f gives the γ_2 strain as long as the layer-parallel shortening is known. To find γ_2 use curves 25(c) or (d), assuming shortening pre- or post-shear. If f lies on the section of line *st* then use the contours marked *st* on Figs. 25(c) or (d) to read off γ_2. If f lies on the section of the line *rs* then use the contours marked *rs*. The curves in Figs. 25(a) and (b) are drawn for oblate strains. For prolate strains use the mirror image of these curves about the $k = 1$ line.

The curves may also be used to construct strain paths and find the finite strains resulting from the superimposition of longitudinal strain and shear strain. For these operations however a simple matrix multiplication and solution method as described briefly by Sanderson *et al.* (1979) may be more suitable.

Note the curves of Figs. 16 and 25 are plotted on the 2-axis Flinn plot (cf. Flinn 1962). The curves representing strain paths thus appear to bounce off the axes of this plot, due to the rapid interchange of axes during strain (cf. Sanderson 1982). An alternative plot would be the 3-axis plot of Nadai (1963) introduced into geology by Hossack (1968). This 3-axis plot is not used here because its main advantages are in interpreting co-axial strain paths (Elliott 1972) and many structural geologists (e.g. Chapman *et al.* 1979) still prefer to publish data on the 2-axis Flinn plot. Thus the 2-axis plot is used here to aid easy comparison with other published data.

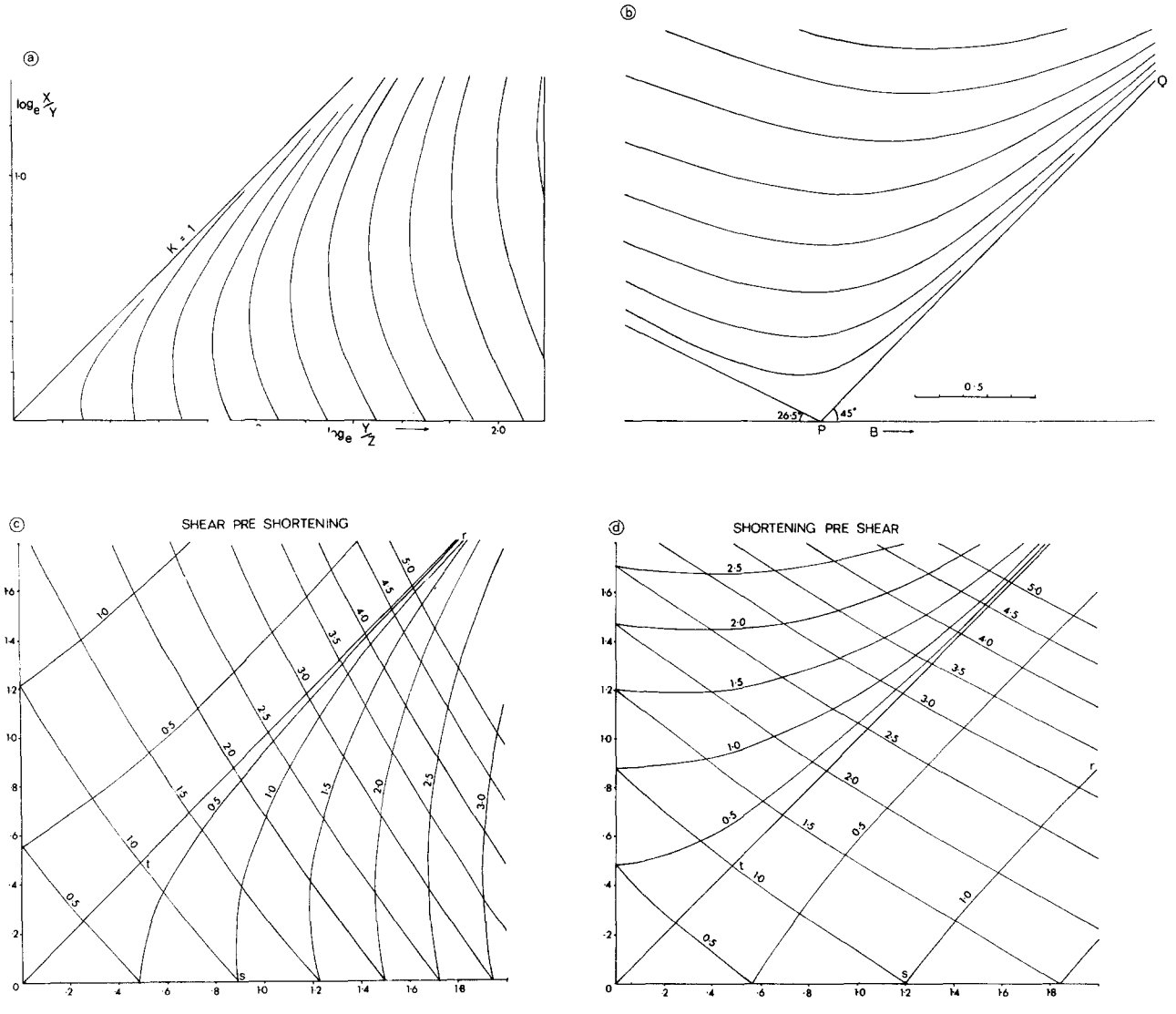

Fig. 25. Curves used for factorizing strain ellipsoids on logarithmic Flinn plot into different components of $\sqrt{\lambda}$, γ_1 and γ_2. See text for details.

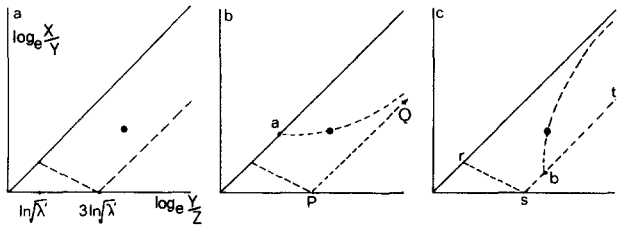

Fig. 26. The procedure for strain factorization. See text for details.